

## Supporting Information

### **A Strategy for Breaking the MOF Template to Obtain Small-Sized and High-Dispersive Polyoxometalate Clusters Loading on the Solid Film**

Jian-Sheng Li, ‡<sup>a</sup> Xiao-Jing Sang, ‡<sup>a</sup> Wei-Lin Chen, \*<sup>a</sup> Lan-Cui Zhang, <sup>b</sup> Zai-Ming Zhu, <sup>b</sup> Yang-Guang Li, \*<sup>a</sup> Zhong-Min Su<sup>a</sup> and En-Bo Wang\*<sup>a</sup>

#### **CONTENTS**

**Section 1 Experimental section**

**Section 2 Supplementary Physical and Chemical Characterizations**

**Section 3 Tables**

## Section 1 Experimental section

### Materials and methods

$\text{K}_6\text{CoW}_{12}\text{O}_{40}$  ( $\text{CoW}_{12}$ )<sup>S1</sup> and MIL-101<sup>S2</sup> were synthesized according to the reported methods, and characterized by UV-vis spectra (Figure S1), TG analysis (Figure S2) and cyclic voltammetry (Figure S3-S4).  $\text{Na}_6\text{H}_2\text{W}_{12}\text{O}_{40}$  ( $\text{H}_2\text{W}_{12}$ ) and all other reagent were purchased commercially and used without further purification.

IR spectra was recorded on an Alpha Centaur FT/IR spectrophotometer with KBr pellets in the range of 400-4000  $\text{cm}^{-1}$  region at room temperature. TG curves were performed on a PerkinElmer TGA7 instrument at a heating rate of 10  $^\circ\text{C min}^{-1}$  from 30 to 600  $^\circ\text{C}$ . X-ray powder diffraction data was collected on a Rigaku D/max-2550 diffractometer using Cu  $K\alpha$  radiation ( $\lambda = 1.5418 \text{ \AA}$ ). The surface photovoltage spectroscopy measurement is carried out on a lab-made instrument, which constitutes a source of monochromatic light, a lock-in amplifier (SR830-DSP) with a light chopper (SR540) and a photovoltaic cell. A 500 W xenon lamp (CHFXQ500 W, Global xenon lamp power) and a double-prism monochromator (Hilger and Watts, D300) provides monochromatic light. The construction of the photovoltaic cell was a sandwich-like structure of ITO–sample–ITO. The nanostructure of the samples were characterized with high resolution transmission electron microscope (HRTEM) (JEOL-2100F) at an acceleration voltage of 200 kV and field emission scanning electron microscopy (FESEM; XL30, FEG, FEI Company) at an accelerating voltage of 25 kV. All photoelectrochemical experiments were performed on a on a CHI601D

electrochemistry station at room temperature equipped with a Xenon lamp as the light source and an AM 1.5 solar filter.

### **Synthesis of CoW<sub>12</sub>@MIL-101**

Tetramethylammonium hydroxide (1.72 g, 25 wt%) was dissolved in 50 mL of deionized water, to which terephthalic acid (1.66g, 10 mmol) was added and followed by stirring for 10 min. Then, [Cr(NO<sub>3</sub>)<sub>3</sub>]·9H<sub>2</sub>O (4.0 g, 10 mmol) was added to the above mixture; Subsequently, K<sub>6</sub>CoW<sub>12</sub>O<sub>40</sub> (4.0 g) was added to the reaction system. The resulting mixture was stirred for 20 min at room temperature. Finally, the obtained mixture was divided into 8 portions and transferred into 13 mL Teflon-lined autoclave and heated at 453 K for 72 h. After cooling to room temperature slowly, the obtained green powder was collected and washed thoroughly with water and DMF by ultrasonic and centrifugation. The product was dried at 60 °C under vacuum.<sup>S3</sup>

### **Synthesis of H<sub>2</sub>W<sub>12</sub>@MIL-101**

The preparation process was similar to that for CoW<sub>12</sub>@MIL-101, except that H<sub>2</sub>W<sub>12</sub> (4.0 g) was used.

### **Preparation of CoW<sub>12</sub>·Cr<sub>2</sub>O<sub>3</sub>@TiO<sub>2</sub>**

The composite was prepared according to a similar process in the literature.<sup>S4</sup> Specifically, 0.05 g of CoW<sub>12</sub>@MIL-101 was dispersed in 5 mL of deionized water by ultrasonic to form mixture A, and 5 mL of isopropyl titanate was dissolved in 3 mL of *n*-butyl alcohol to form solution B; then mixture A was added to solution B dropwise under vigorous stirring. Subsequently, the resulting turbid solution was stirred at 45 °C for 3 h and 80 °C for another 3 h. The obtained hydrogel was

transferred into the vacuum oven and maintained at 45 °C for 12 h followed by 80 °C for 3 h. After washing and drying, the powder was calcined at 450 °C for 30 min.  $\text{H}_2\text{W}_{12}\cdot\text{Cr}_2\text{O}_3@\text{TiO}_2$  was prepared with the similar method by replacing  $\text{CoW}_{12}@\text{MIL-101}$  with  $\text{H}_2\text{W}_{12}@\text{MIL-101}$ .

For comparison,  $\text{CoW}_{12}@\text{TiO}_2$  and  $\text{Cr}_2\text{O}_3@\text{TiO}_2$  were also prepared to assemble QDSCs. Their synthesis processes were similar to that of  $\text{CoW}_{12}\cdot\text{Cr}_2\text{O}_3@\text{TiO}_2$ , except using bulk  $\text{CoW}_{12}$  powder and MIL-101 powder to replace  $\text{CoW}_{12}@\text{MIL-101}$  during the process.

### **Quantum dot sensitized solar cells fabrication**

The water-soluble mercaptopropionic acid-capped CdSe quantum dot (MPA-CdSe) was prepared according to the reported method by Zhong et al.<sup>S5</sup> The reference cells with un-doped photoanodes sensitized by CdSe were denoted as QDSCs. The solar cell assembly process was illustrated in Fig. S6.

The  $\text{TiO}_2$  paste was prepared as follows: 0.3 g of  $\text{CoW}_{12}\cdot\text{Cr}_2\text{O}_3@\text{TiO}_2$  powder and 1.7 g of P25 was added to 15.2 mL of anhydrous ethanol under sonication consecutively. After sonication for 30 min, 8.1 g of terpineol and 10.4 g of an ethanol solution with 10 wt% EC were added to the mixture and sonicated for more 30 min. Finally, the paste was obtained by removing ethanol under stirring. The final fabricated cells were denoted as  $\text{CoW}_{12}\cdot\text{Cr}_2\text{O}_3@\text{TiO}_2/\text{QDSC}$ .

Other kinds of paste was prepared according to the similar process.<sup>S6</sup> And the corresponding cells were denoted as  $\text{CoW}_{12}@\text{TiO}_2/\text{QDSC}$  and  $\text{Cr}_2\text{O}_3@\text{TiO}_2/\text{QDSC}$  respectively.

The photoanode film was prepared by screen-printing<sup>S7</sup> TiO<sub>2</sub> paste on the FTO glass which had been cleaned and pretreated by 40 mmol L<sup>-1</sup> TiCl<sub>4</sub> at 70 °C for 30 min. Five layers of paste was deposited on the FTO glass to control the thickness of TiO<sub>2</sub> working electrode. Layers were then sintered at 325 °C for 5 min, 375 °C for 5 min, and 450 °C for 30 min. Subsequently, the resulting films were post-treated in 40 mmol L<sup>-1</sup> TiCl<sub>4</sub> solution for 30 min at 70 °C and calcined in air at 450 °C for 30 min again. When cooled to room temperature, the film was coated with CdSe by immersing the film in MPA-CdSe aqueous solution for 4 h, followed by rinsing with water and drying with N<sub>2</sub>. After finishing sensitization, the sensitized TiO<sub>2</sub> film was coated with ZnS by twice dipping alternately into 0.1 M Zn(OAc)<sub>2</sub> and 0.1 M Na<sub>2</sub>S solutions for 1 min/dip.

The electrolyte is composed of 2.0 M Na<sub>2</sub>S, 2.0 M S and 0.2 M KCl in methanol/water (3:7, v/v) solution. The Cu<sub>2</sub>S counter electrode was prepared by immersing the polished brass in concentrated HCl at 70 °C for 5 min and soaking it in the polysulfide electrolyte for 10min, followed by washing with deionized water and drying with N<sub>2</sub>.

The solar cells were assembled by sandwiching a Cu<sub>2</sub>S counter electrode and a quantum dot sensitized photoanode using a about 50- $\mu$ m thickness scotch spacer, then the above electrolyte was introduced between the electrodes by the capillary action.<sup>S4</sup>

## Section 2 Supplementary Physical and Chemical Characterizations

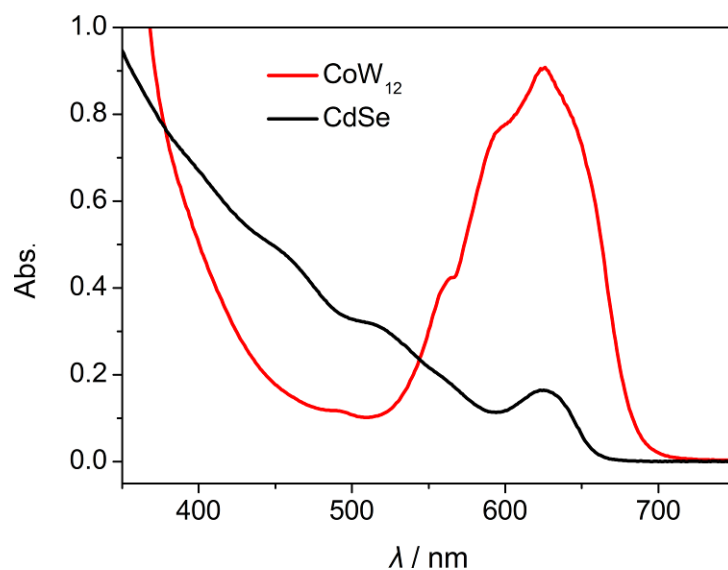


**Figure S1** UV-vis absorption spectrum of CoW<sub>12</sub> and CdSe aqueous solution. Compared with CdSe, CoW<sub>12</sub> also displayed visible characteristic peak centering at 625 nm with stronger absorption.

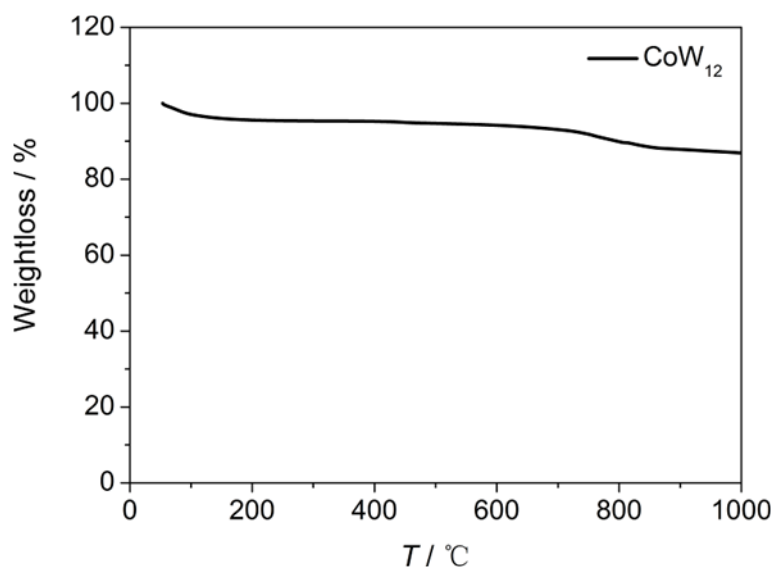


**Figure S2** TG curve of CoW<sub>12</sub>. The thermal stability of CoW<sub>12</sub> was analyzed by its TG curve, which displayed three-step weightlosses occurred in the temperature range of 50-1000 °C. The three-step weightlosses were all attributed to the loss of water,

demonstrating that the skeleton structure of  $\text{CoW}_{12}$  remained during the temperature range. Therefore,  $\text{CoW}_{12}$  was stable after sintering.

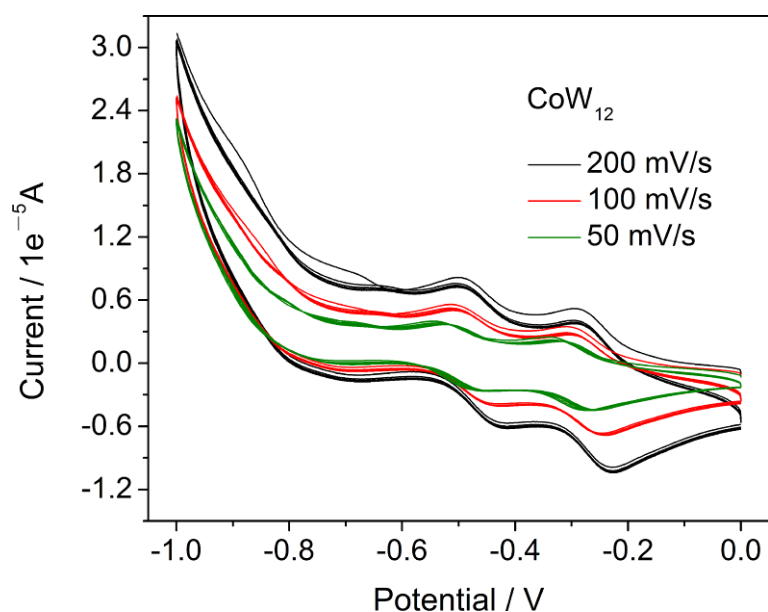


**Figure S3** The cyclic voltammogram of  $\text{CoW}_{12}$  in  $\text{Na}_2\text{SO}_4/\text{H}_2\text{SO}_4$  solution

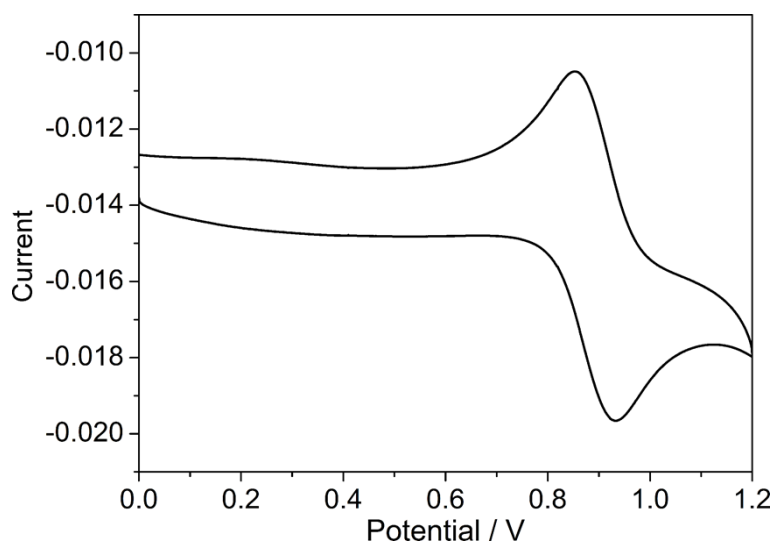


**Figure S4** The cyclic voltammogram of  $\text{CoW}_{12}$  in the potential range from 0 V to 1.2 V. As can be seen, there was a pair of reversible redox peak located at 0.93 V and 0.85 V, respectively, which was assigned to the oxidation of  $\text{Co}^{\text{II}}$  to  $\text{Co}^{\text{III}}$  and its reduction process.

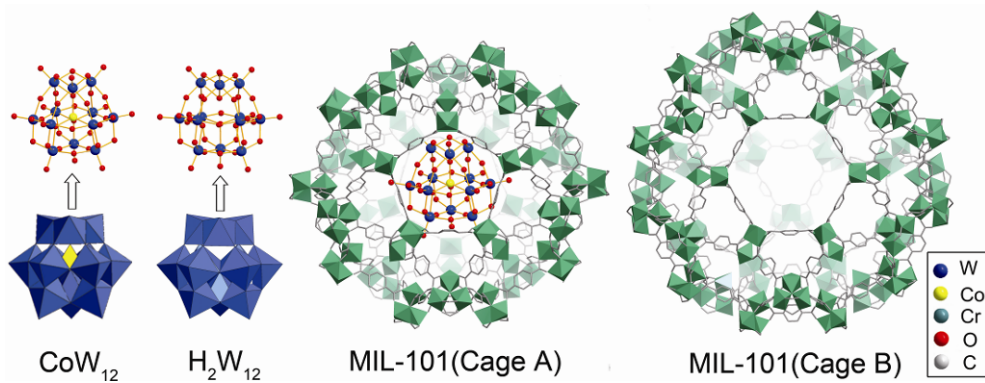


**Figure S5** The structures of  $\text{CoW}_{12}$ ,  $\text{H}_2\text{W}_{12}$  and MIL-101

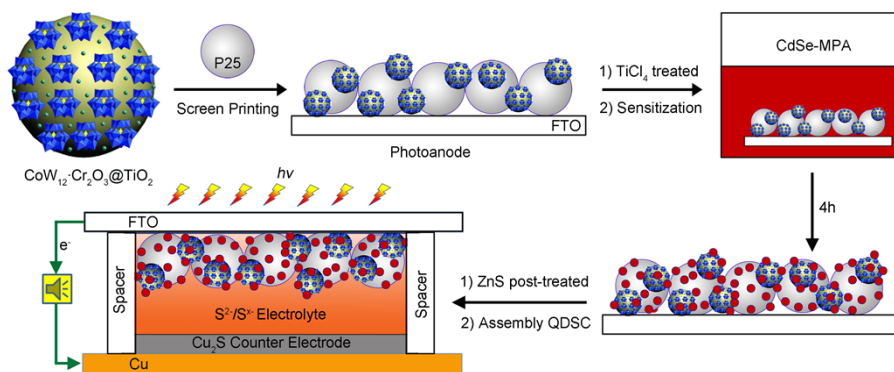


**Figure S6** The schematic assembly process of quantum dot sensitized solar cells

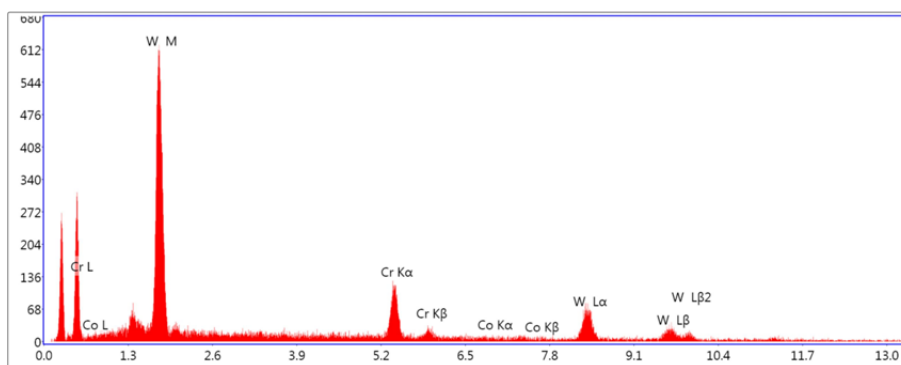


**Figure S7** EDS spectrum for  $\text{CoW}_{12}@\text{MIL-101}$

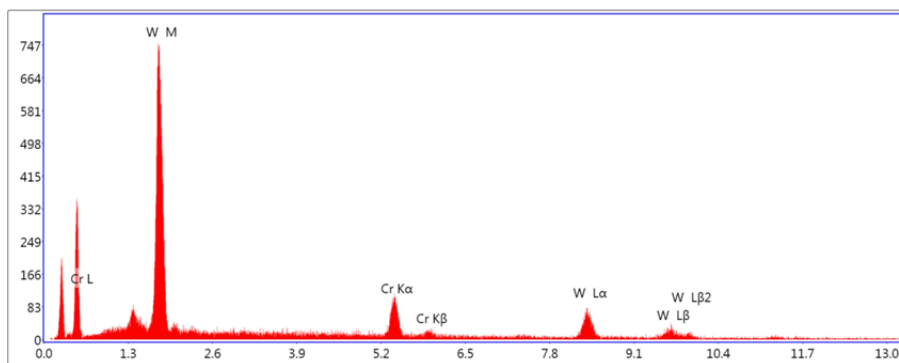


**Figure S8** EDS spectrum for  $\text{H}_2\text{W}_{12}@MIL-101$

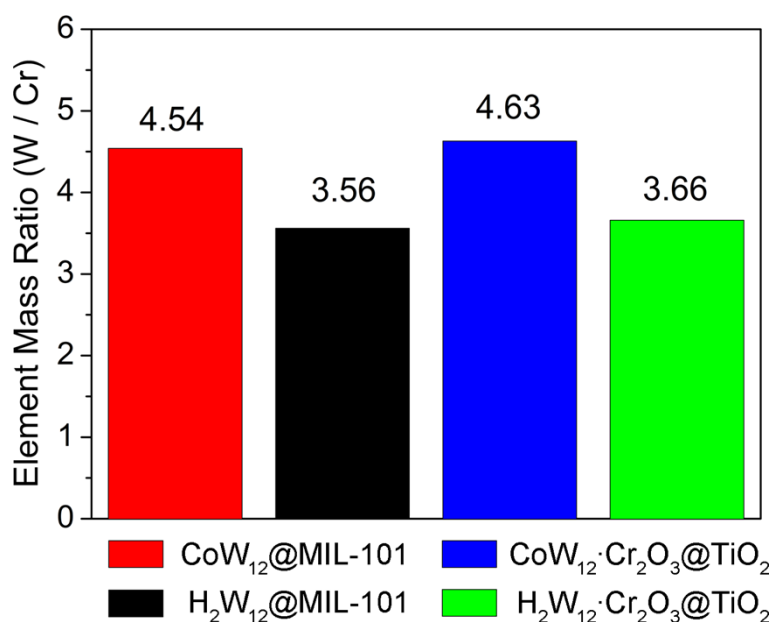


**Figure S9** The elemental mass ratio of W/Cr in  $\text{CoW}_{12}@MIL-101$  (red rectangular),  $\text{H}_2\text{W}_{12}@MIL-101$  (dark rectangular),  $\text{CoW}_{12}\cdot\text{Cr}_2\text{O}_3@TiO_2$  (blue rectangular) and  $\text{H}_2\text{W}_{12}\cdot\text{Cr}_2\text{O}_3@TiO_2$  (green rectangular)

The loading amount of POMs in  $\text{POM}@MIL-101$  was determined by the elemental analysis, from which the W content in  $\text{CoW}_{12}@MIL-101$  and  $\text{H}_2\text{W}_{12}@MIL-101$  was 25.39% and 23.64%, respectively. Based on both the elemental analysis result and molecular weight of  $\text{K}_6\text{CoW}_{12}\text{O}_{40}$  ( $3138.5 \text{ g mol}^{-1}$ ) and  $\text{Na}_6\text{H}_2\text{W}_{12}\text{O}_{40}$  ( $2985.6 \text{ g mol}^{-1}$ ), the content of  $\text{CoW}_{12}$  and  $\text{H}_2\text{W}_{12}$  in  $\text{CoW}_{12}@MIL-101$  and  $\text{H}_2\text{W}_{12}@MIL-101$  can be calculated according to the formula:  $\text{POMs} (\mu\text{mmol g}^{-1}) = 1 \times 10^6 (\text{W content in the$

hybrid material, %)/(MW<sub>POM</sub> × W content in POMs).<sup>S8</sup> Accordingly, the estimated loading amount of CoW<sub>12</sub> and H<sub>2</sub>W<sub>12</sub> in CoW<sub>12</sub>@MIL-101 and H<sub>2</sub>W<sub>12</sub>@MIL-101 was 115.1 μmmol g<sup>-1</sup> and 107.2 μmmol g<sup>-1</sup>, or 36.12wt% and 32.05wt%, respectively. Furthermore, the ratio of W/Cr in CoW<sub>12</sub>@MIL-101 (4.54) was consistent with that of CoW<sub>12</sub>·Cr<sub>2</sub>O<sub>3</sub>@TiO<sub>2</sub> (4.63).

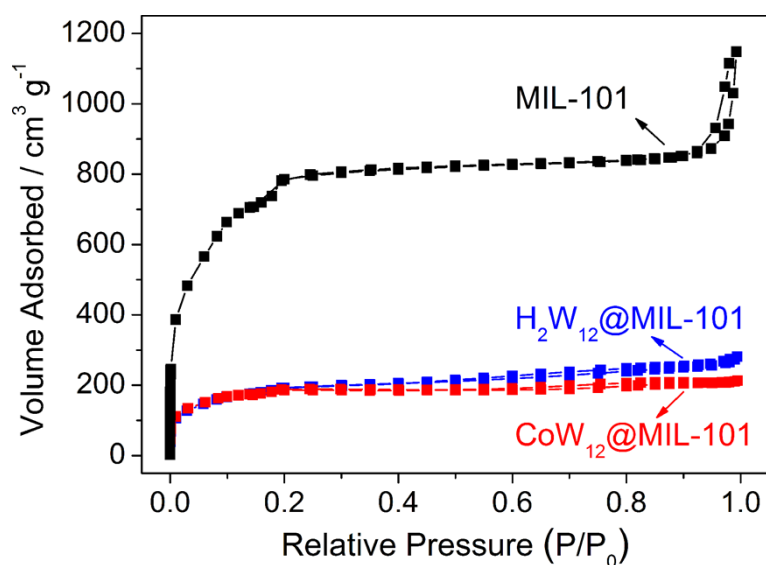
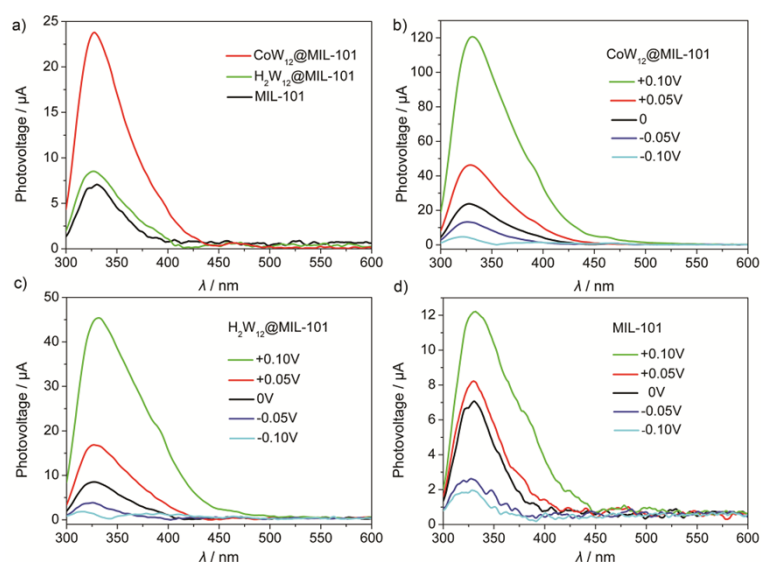


Figure S10 Nitrogen adsorption-desorption isotherms at -196 °C for MIL-101 (dark), CoW<sub>12</sub>@MIL-101 (red) and H<sub>2</sub>W<sub>12</sub>@MIL-101 (blue)

The nitrogen isotherms of MIL-101 with and without included POMs were performed to compare the porosity of MIL-101 and POMs@MIL-101 shown in Fig. S10. As can be concluded, MIL-101 gives a BET surface area and a pore volume of 2840 m<sup>2</sup> g<sup>-1</sup> and 1.41 cm<sup>3</sup> g<sup>-1</sup>; whereas, CoW<sub>12</sub>@MIL-101 had the lower BET surface area (660 m<sup>2</sup> g<sup>-1</sup>) and pore volume (0.32 cm<sup>3</sup> g<sup>-1</sup>); similarly, H<sub>2</sub>W<sub>12</sub>@MIL-101 showed the lower BET surface area (692 m<sup>2</sup> g<sup>-1</sup>) and pore volume (0.41 cm<sup>3</sup> g<sup>-1</sup>), which was attributed to the inclusion of POMs into the pores of MIL-101 to occupy the pore space. Moreover, their average pore size were estimated according to the

BJH (Barrett-Joyner-Halenda) method based on nitrogen adsorption isotherms (Table S1). As can be concluded, both  $\text{CoW}_{12}@MIL-101$  and  $\text{H}_2\text{W}_{12}@MIL-101$  showed smaller average pore size than that of MIL-101.



**Figure S11** a) SPS of  $\text{CoW}_{12}@MIL-101$  (red line),  $\text{H}_2\text{W}_{12}@MIL-101$  (green line) and MIL-101 (dark line) at the bias of 0 V; EFISPS of b)  $\text{CoW}_{12}@MIL-101$ ; c)  $\text{H}_2\text{W}_{12}@MIL-101$  and d) MIL-101

The surface photovoltage spectroscopy (SPS) was carried out study the charge transfer process of POM-based MOF materials. The SPS presents the change of the surface potential barrier of the measured materials under light illumination, which not only relates to the electron transitions upon excitation but also reflects their separation and transfer process. As depicted in Figure S11a, both MIL-101 and  $\text{POM}@MIL-101$  displayed significant surface photovoltage from 300 to 400 nm upon optical inducement, indicating they exhibited semiconductor characteristic and produced electron-hole separation. In addition,  $\text{CoW}_{12}@MIL-101$  exhibited much stronger SPS intensity as well as wider spectrum response range, indicating charge transfer between

MIL-101 framework and  $\text{CoW}_{12}$  existed. The electric-field-induced surface photovoltage spectroscopy (EFISPS) could be measured by applying an external electric field to the sample. As shown in Figure S11b-11d, the SPS response of both MIL-101 and  $\text{POM@MIL-101}$  increased after a positive external voltage was applied. Alternatively, a negative external electric field resulted in the reduced SPS intensity. These results suggested that these compounds take the character of a *p*-type material because the direction of the built-in field for the *p*-type material coincides with that of a positive external electric field, which could increase the photo-generated electron-hole pairs separation and enhance the SPS response accordingly.

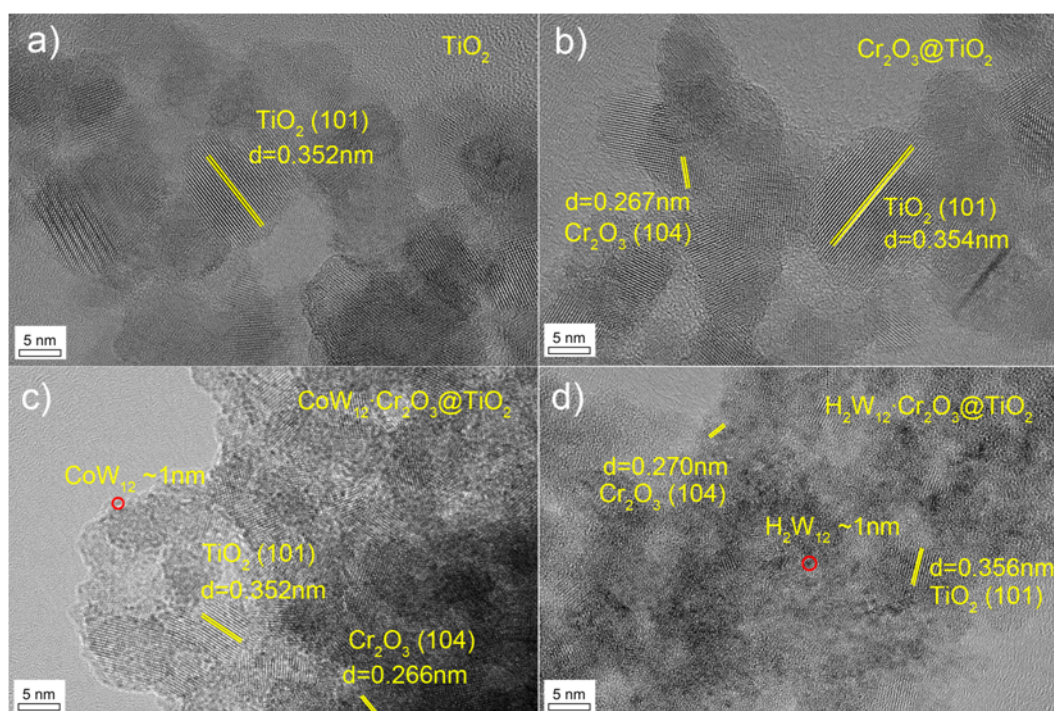


**Figure S12** HRTEM images of a)  $\text{TiO}_2$ , b)  $\text{Cr}_2\text{O}_3@\text{TiO}_2$ , c)  $\text{CoW}_{12}\cdot\text{Cr}_2\text{O}_3@\text{TiO}_2$  and d)  $\text{H}_2\text{W}_{12}\cdot\text{Cr}_2\text{O}_3@\text{TiO}_2$  powder

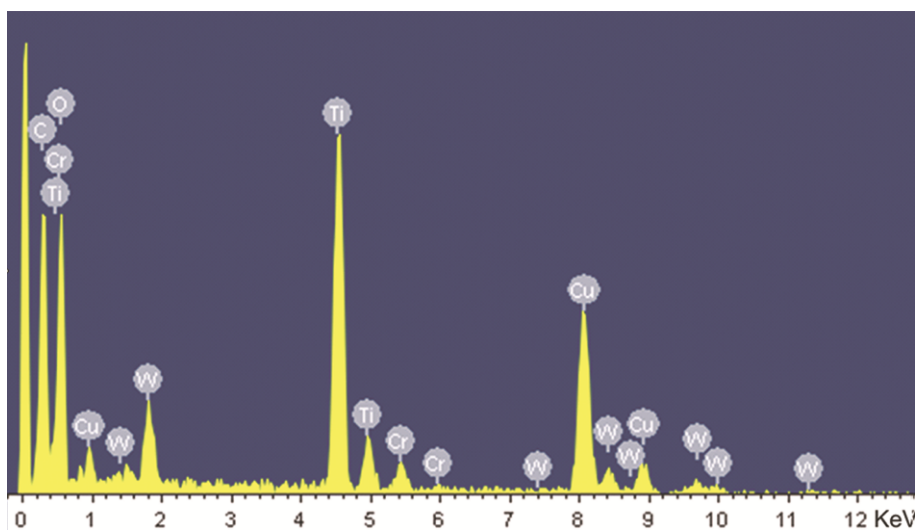


**Figure S13** EDS analysis of  $\text{CoW}_{12}\cdot\text{Cr}_2\text{O}_3@\text{TiO}_2$  powder

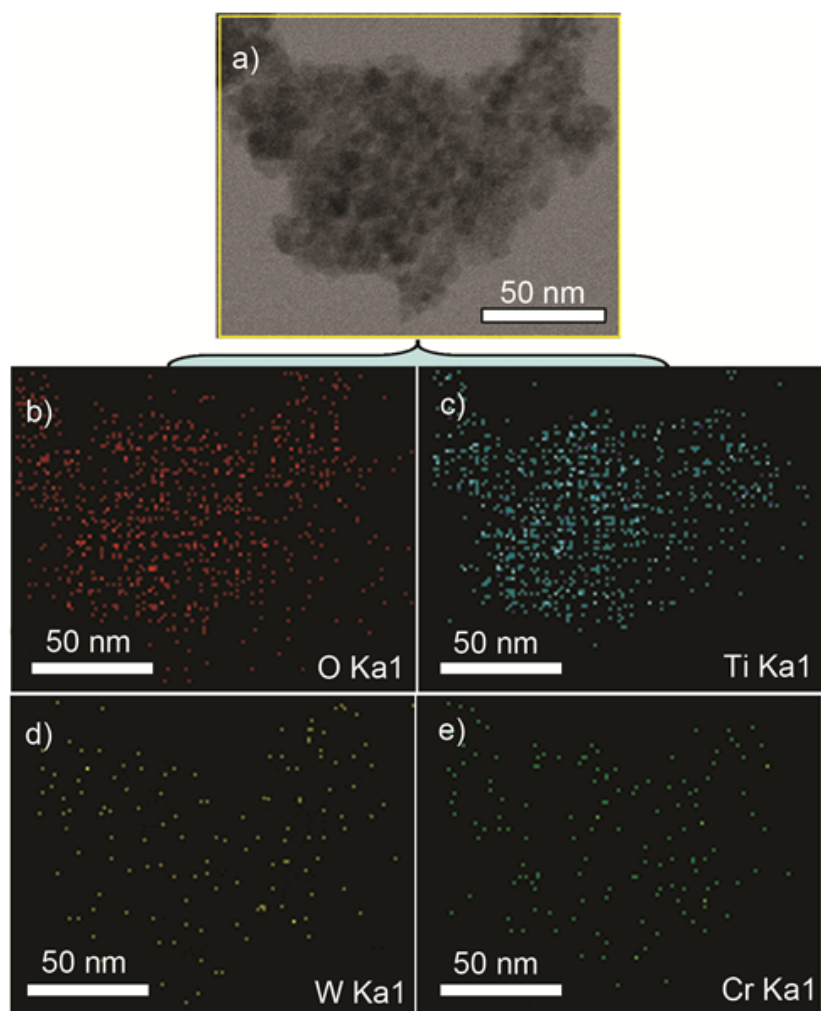


**Figure S14** Element mapping of  $\text{CoW}_{12}\cdot\text{Cr}_2\text{O}_3@\text{TiO}_2$  powder

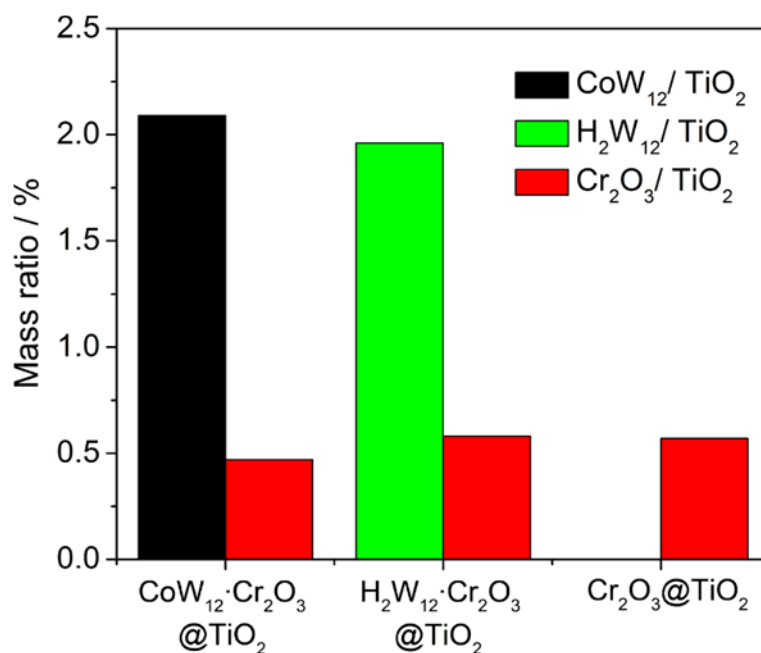


**Figure S15** The mass ratio of POMs and Cr<sub>2</sub>O<sub>3</sub> to TiO<sub>2</sub> in the composite

POM·Cr<sub>2</sub>O<sub>3</sub>@TiO<sub>2</sub>

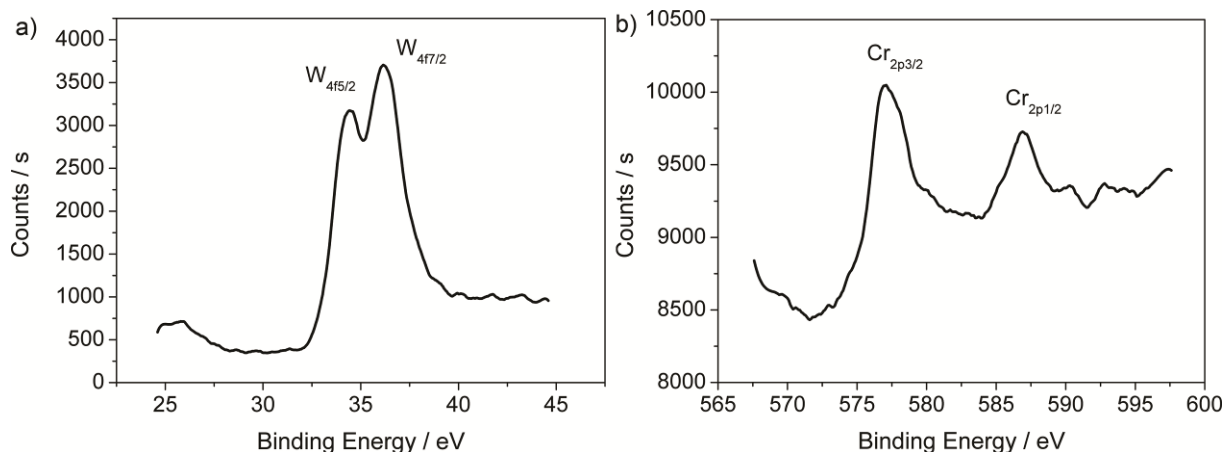


**Figure S16** XPS spectra of CoW<sub>12</sub>·Cr<sub>2</sub>O<sub>3</sub>@TiO<sub>2</sub> for: a) W and b) Cr element

The oxidation states of W and Cr atoms in the composite were characterized by XPS. The binding energy located at 34.6 and 36.2 eV in Figure S16a was ascribed to W<sub>4f</sub> of CoW<sub>12</sub>, which corresponded to the W<sup>VI</sup> oxidation state and suggested POM anions existed in form of the oxidized state. The XPS spectrum for Cr<sub>2p</sub> (Figure S16b) showed two peaks at ca. 577.0 eV and 586.9 eV in the energy region of Cr<sub>2p<sub>3/2</sub></sub> and Cr<sub>2p<sub>1/2</sub></sub> separately, which corresponded to the Cr<sup>III</sup> oxidation state.

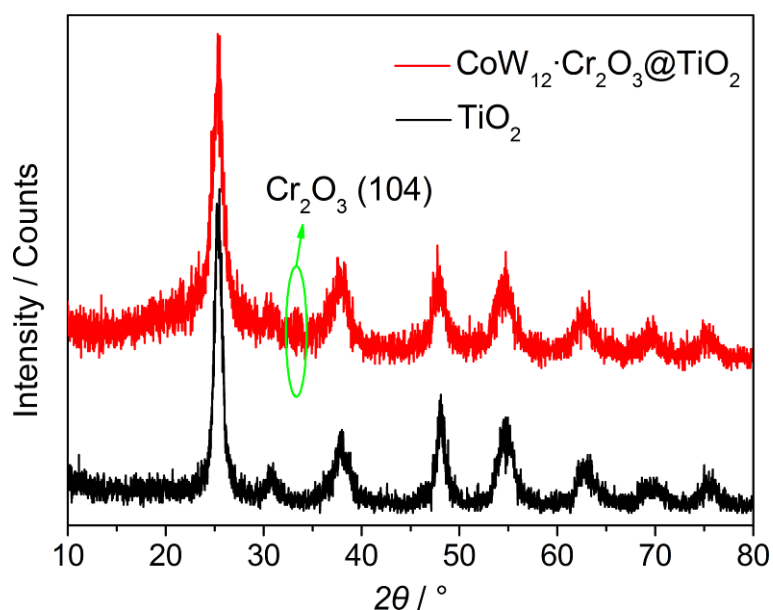


**Figure S17** Powder X-ray diffraction of  $\text{TiO}_2$  (dark line) and  $\text{CoW}_{12}\cdot\text{Cr}_2\text{O}_3@\text{TiO}_2$  (red line) powder

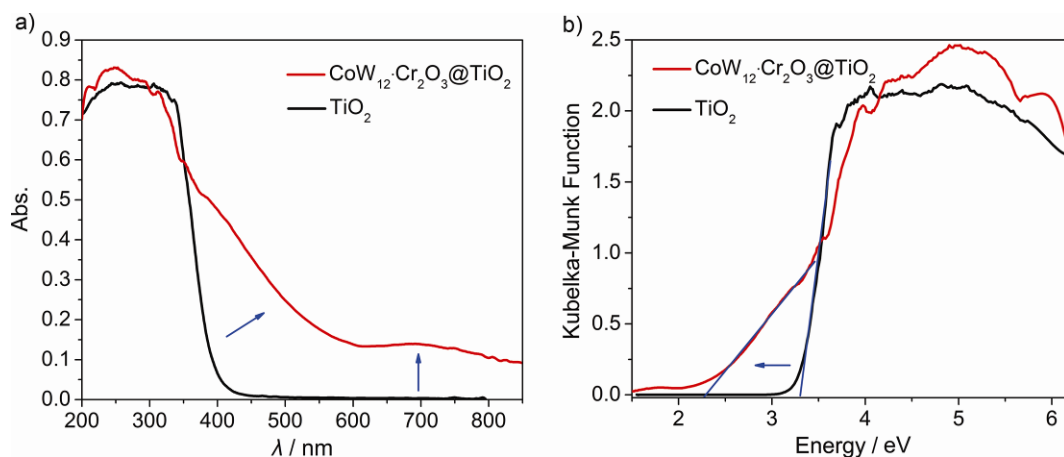


**Figure S18** a) The solid diffuse absorption spectra of pure  $\text{TiO}_2$  (dark line) and  $\text{CoW}_{12}\cdot\text{Cr}_2\text{O}_3@\text{TiO}_2$  (red line) powder; b) Their plots of K-M function against energy

E

In contrast with  $\text{TiO}_2$ ,  $\text{CoW}_{12}\cdot\text{Cr}_2\text{O}_3@\text{TiO}_2$  displayed wider spectrum absorption which covered the whole of UV, visible and near-infrared region. Their band gap could be determined by the plot of Kubelka-Munk function  $F$  against energy  $E$ , from which  $E_g$  of  $\text{CoW}_{12}\cdot\text{Cr}_2\text{O}_3@\text{TiO}_2$  was estimated as 2.3 eV by the intersection point

between the energy axis and the line extrapolated from the linear portion of the absorption edge. Compared with the band gap of  $\text{TiO}_2$  (3.3 eV), the composites possessed more efficient spectrum utilization.

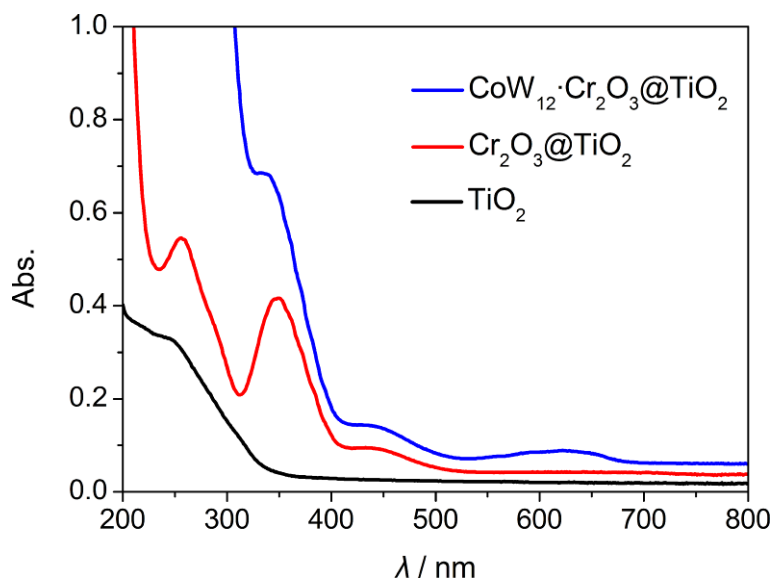


**Figure S19** UV-vis absorption spectra of aqueous solution desorbed from  $\text{TiO}_2$  (dark line),  $\text{Cr}_2\text{O}_3@\text{TiO}_2$  (red line) and  $\text{CoW}_{12}\cdot\text{Cr}_2\text{O}_3@\text{TiO}_2$  (blue line)

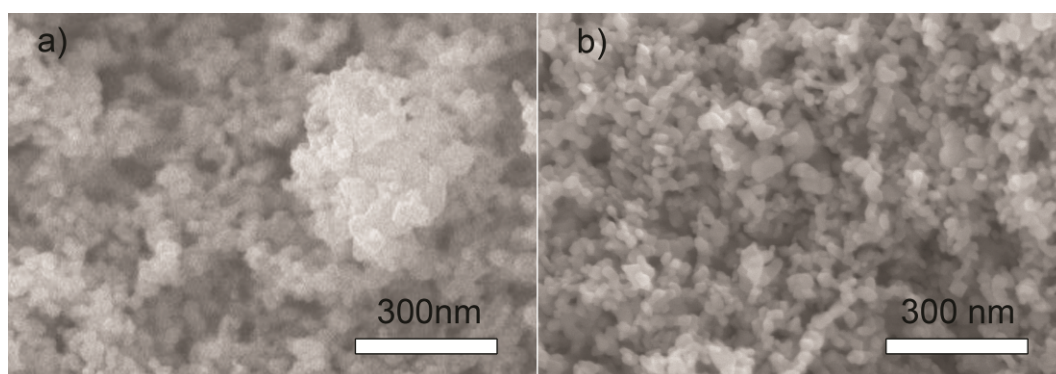


**Figure S20** SEM images of different photoanode films: a)  $\text{CoW}_{12}\cdot\text{Cr}_2\text{O}_3@\text{TiO}_2$ -doped film; b) pure P25 film

Figure S20 depicted the SEM images of two kinds of photoanode films, which showed that pure P25 film consisted of uniform  $\text{TiO}_2$  particles, whereas  $\text{CoW}_{12}\cdot\text{Cr}_2\text{O}_3@\text{TiO}_2$ -doped film contained some aggregates.

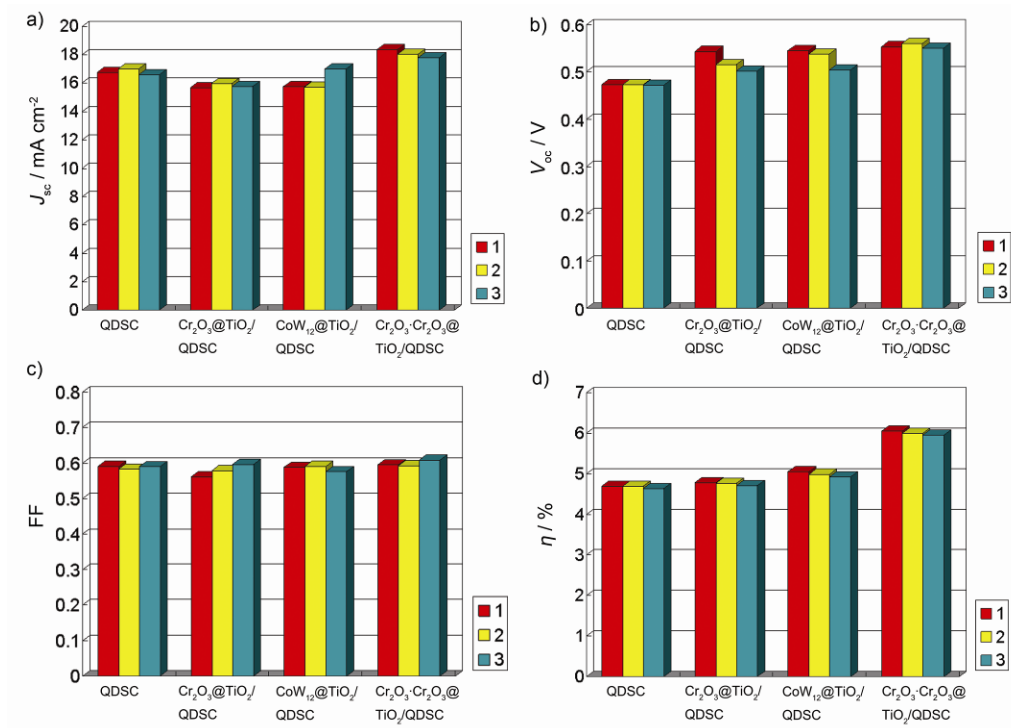


**Figure S21** The photovoltaic characteristics for three sets of QDSCs using various photoanodes with CdSe sensitizer

### Section 3 Tables

Table S1. BET surface area, Langmuir surface area, total pore volume and average pore size for the studied samples

Sample	BET SA / m <sup>2</sup> g <sup>-1</sup>	Langmuir SA / m <sup>2</sup> g <sup>-1</sup>	Pore Volume /m <sup>3</sup> g <sup>-1</sup>	Pore Size / nm
MIL-101	2840	3934	1.41	4.20
H <sub>2</sub> W <sub>12</sub> @MIL-101	692	947	0.41	3.87
CoW <sub>12</sub> @MIL-101	660	895	0.32	3.11

Table S2. Photovoltaic parameters of QDSCs with different photoanodes sensitized by CdSe

Cells	$J_{sc}$ / mA cm <sup>-2</sup>	$V_{oc}$ / V	FF	$\eta$ / %	Average / %
QDSC	16.77	0.473	0.591	4.69	4.67±0.04
	17.01	0.473	0.583	4.69	
	16.58	0.472	0.590	4.63	
Cr <sub>2</sub> O <sub>3</sub> @TiO <sub>2</sub> /QDSC	15.69	0.543	0.561	4.78	4.75±0.04
	15.98	0.515	0.578	4.76	
	15.77	0.501	0.596	4.71	
CoW <sub>12</sub> @TiO <sub>2</sub> /QDSC	15.76	0.545	0.588	5.05	4.99±0.06
	15.71	0.537	0.591	4.99	
	16.99	0.504	0.576	4.93	
CoW <sub>12</sub> ·Cr <sub>2</sub> O <sub>3</sub> @TiO <sub>2</sub> /QDSC	18.38	0.553	0.595	6.05	6.00±0.05
	18.05	0.560	0.593	6.00	
	17.80	0.550	0.608	5.95	

## References

- S1 A. L. Nolan, R. C. Burns and G. A. Lawrance, *J. Chem. Soc., Dalton Trans.*, 1998, 3041.
- S2 J. F. Yang, Q. Zhao, J. P. Li and J. X. Dong, *Micropor. Mesopor. Mat.*, 2010, **130**, 174.
- S3 A. X. Yan, S. Yao, Y. G. Li, Z. M. Zhang, Y. Lu, W. L. Chen and E. B. Wang, *Chem. Eur. J.*, 2014, **20**, 6927.
- S4 L. Li, Y. L. Yang, R. Q. Fan, X. Wang, Q. M. Zhang, L. Y. Zhang, B. Yang, W. W. Cao, W. Z. Zhang, Y. Z. Wang and L. Q. Ma, *Dalton Trans.*, 2014, **43**, 1577.
- S5 H. Zhang, K. Cheng, Y. M. Hou, Z. Fang, Z. X. Pan, W. J. Wu, J. L. Hua and X. H. Zhong, *Chem. Commun.*, 2012, **48**, 11235.
- S6 Z. L. Du, H. Zhang, H. L. Bao and X. H. Zhong, *J. Mater. Chem. A*, 2014, **2**, 13033.
- S7 S. Ito, P. Chen, P. Comte, M. K. Nazeeruddin, P. Liska, P. Péchy and M. Grätzel, *Prog. Photovolt: Res. Appl.*, 2007, **15**, 603.
- S8 L. H. Wee, F. Bonino, C. Lamberti, S. Bordiga and J. A. Martens, *Green Chem.*, 2014, **16**, 1351.